# Wireless Backhaul Strategies for Real-Time High-Density Seismic Acquisition

Varun Amar Reddy, Gordon L. Stüber
Center for Energy and Geo Processing
School of Electrical & Computer Engineering
Georgia Institute of Technology
Atlanta, GA 30332, USA
varun.reddy@gatech.edu, stuber@ece.gatech.edu

Suhail Al-Dharrab, Ali Hussein Muqaibel, Wessam Mesbah
Center for Energy and Geo Processing
Electrical Engineering Department
King Fahd University of Petroleum & Minerals
Dhahran 31261, Saudi Arabia
{suhaild, muqaibel, mesbahw}@kfupm.edu.sa

***Abstract*—Modern geophysics methods for oil and gas exploration are able to generate subsurface images of superior quality and depth, albeit making real-time data acquisition a more challenging task. While current literature addresses data transfer issues primarily between the geophones and the gateway nodes, a communication scheme for the transfer of data from the gateway nodes to the sink largely remains unsolved. A novel wireless geophone network architecture for seismic data acquisition is described, with the objective of eliminating cable-based systems and providing Gigabit rates in order to support real-time acquisition. A performance analysis is conducted for various mesh networks employing IEEE 802.11ac, IEEE 802.11ad, and free space optical communication, from the geophysics perspective. Our findings suggest that the bottleneck links can be shifted from the top to the bottom of existing architectures, and a scalable approach requiring minimal number of gateway devices can be designed for high-density seismic surveys.**

## I. Introduction

Oil and gas prospectors conduct seismic surveys over areas as large as 100 $km^2$ to generate images of the subsurface of the Earth, using which the desired resources can be extracted. Vibroseis trucks are used to generate seismic waves, termed as a *sweep*, that travel into the ground and are reflected by subsurface layers. The reflected waves are recorded by a large number of devices called *geophones*, which record data and transfer it to the *Data Collection Center (DCC)* for subsequent processing [1], [2].

The motivation for employing wireless data acquisition arises from the typical present-day use of cable to interconnect nearly 10,000-30,000 geophones. Eliminating the use of cable presents a significant reduction in the overall equipment weight and related logistics costs. Wireless acquisition also enables larger and denser deployments, which can help create subsurface images of superior quality.

A challenge with wireless systems is achieving real-time seismic data acquisition at the DCC, which would allow the field engineers to adaptively modify the nature of subsequent sweeps based on the data obtained from the current sweep [3]. For instance, the sweep parameters can be modified as per conditions that may differ across various sections in the survey area. Quality control information can also be obtained in real-time in order to detect faulty geophones. The use of autonomous or nodal systems presents a simpler approach wherein data is buffered over long periods of time and manually collected at a later stage. However, this would compromise on the aforementioned benefits of a real-time acquisition system.

Given a sampling time of 0.5 ms, a three-component geophone equipped with a 24-bit analog-to-digital converter would generate data at a rate of 144 kbps. Seismic surveys in the future are projected to deploy up to 100,000 geophones, thereby requiring data transfer rates on the order of several Gigabits per second. Although LTE or 5G networks are attractive options, their licensed nature and lack of available channel bandwidth limit their use. Low power wide area networks and *MulteFire* [4], a standalone unlicensed version of LTE, offer promising solutions in terms of the power consumption and range, but cannot support data rates on the order of several Gigabits per second.

Prior works in literature follow a relatively common approach wherein data from a cluster of geophones is aggregated at storage units, from where it is relayed towards the DCC. Data communication techniques at the lowest level between the geophones and the storage units have been studied extensively and differ largely among previous works – ultra-wideband (UWB) with distributed beaconing [5], IEEE 802.11 mesh with TDMA/FDMA [6], IEEE 802.11af star topology [7], [8], IEEE 802.11ad with adaptive formation of personal basic service sets (PBSS) [9]. However, the communication methodology at the DCC has not received as much attention, and a common choice across the previous works for the communication protocol between the storage units and the DCC is some variant of an IEEE 802.11n/ac mesh network.

Such an IEEE 802.11n/ac mesh network would not be able to support real-time acquisition on the order of several Gbps at the DCC. Moreover, the precise communication methodology for such a mesh network has not been studied in [5], [6]. In this work, a novel wireless geophone network architecture is proposed in order to address the need for high-rate wireless backhauls towards the DCC. The network topology is

This work is supported by the Center for Energy and Geo Processing at Georgia Institute of Technology and King Fahd University of Petroleum and Minerals, under grant number GTEC1601.

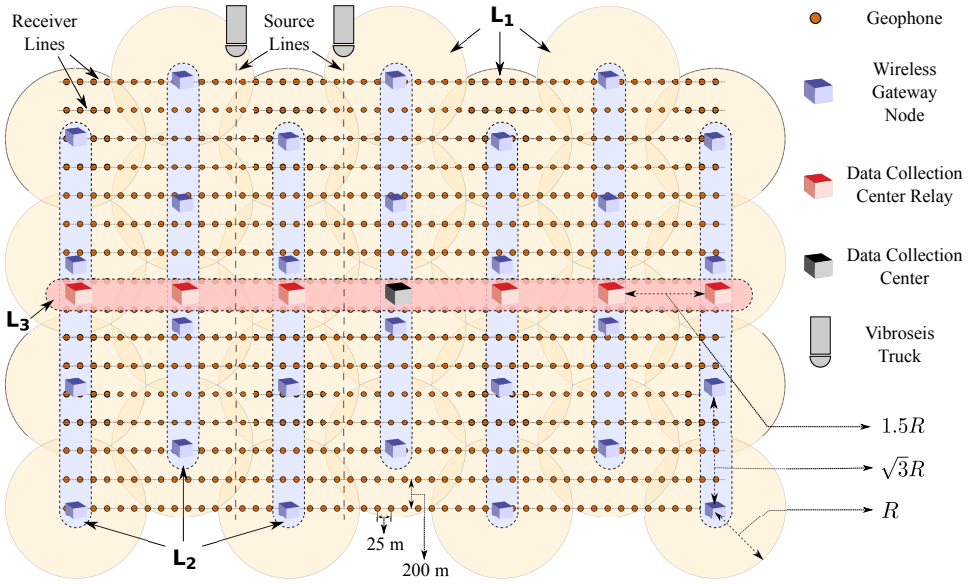


Fig. 1: A Hierarchical Architecture for Seismic Acquisition.

determined after taking into the account the seismic acquisition requirements and the impact of co-channel interference. Schemes based on the use of Unmanned Aerial Vehicles (UAVs), the IEEE 802.11ad standard, and free-space optical communication are assessed and compared with the IEEE 802.11ac standard. A performance evaluation is conducted from the seismic acquisition standpoint, and the number of requisite gateway nodes is determined as a function of latency.

## II. Proposed Network Architecture

Vibroseis trucks move along *Source Lines (SLs)* and generate a sweep for a duration of 8-10 s called the *sweep length* ($\mathcal{S}$). The geophones are laid out along *Receiver Lines (RLs)*, and record the reflected seismic waves subsequently after the sweep length, for a duration of 6-8 s called the *listen interval* ($\mathcal{L}$). *Flip-flop* operation is a popularly used technique which imposes a time constraint for $(\mathcal{L}+\mathcal{S})$ for real-time acquisition [2].

An orthogonal geometry is considered [1], wherein the RLs and SLs are perpendicular to one another. An illustration of the proposed architecture is shown in Fig. 1, in which the geophones are positioned 25 m apart and the RLs are 200 m apart, over an area of 72 km$^2$. The bottommost layer of the architecture, $\mathbf{L_1}$, consists of the links between *Wireless Gateway Nodes (WGNs)* and the geophones. In this analysis, the $\mathbf{L_1}$ layer parameters are derived from [8] where the WGNs are deployed in a hexagonal tessellating pattern. The next layer of the architecture, $\mathbf{L_2}$, is responsible for data transfer from the WGNs to the nearest *DCC Relay (DCCR)*. Directional antennas are employed in parallel to the SLs so as to circumvent the obstructions created by the vibroseis trucks. The topmost layer of the architecture, $\mathbf{L_3}$, represents the bottleneck links between the DCCRs and the DCC.

## III. Wireless Backhaul Strategies

A variety of wireless backhaul strategies are proposed to tackle the data rate requirements at the $\mathbf{L_2}$ and $\mathbf{L_3}$ layers. The underlying principle behind the proposed schemes is that the use of a multi-channel mesh network can significantly improve network capacity and achieve the requisite data rates to observe real-time acquisition. Assuming that each node is supported by two interfaces, each adjacent pair of nodes can operate on a unique channel. However, this method of frequency reuse will introduce co-channel interference that can hamper the communication performance. The aforementioned aspects are elucidated in the following sections.

### A. IEEE 802.11ac Mesh Network

The IEEE 802.11ac standard can provide data rates up to 500 Mbps over a channel bandwidth of 80 MHz [10]. In the case of seismic data acquisition, a link budget analysis reveals that a large EIRP is desirable, given the large distances of $\sqrt{3}R$ and $1.5R$ at layers $\mathbf{L_2}$ and $\mathbf{L_3}$ respectively, where $R$ is the WGN cell radius defined as the distance from the center to the corner of the hexagon. The various link budget parameters

TABLE I: Parameters for IEEE 802.11ac

| Symbol | Parameter | Value |
|---|---|---|
| $P_t$ | Transmit Power | 16 dBm |
| $G$ | Realized Antenna Gain | 14 dB |
| $f$ | Operating Frequency | 5.250-5.805 GHz |
| $h$ | Antenna Height | 2-3 m |
| $d$ | Distance between Adjacent Nodes | 300-1400 m |
| $k_B$ | Boltzmann Constant | $1.38 \times 10^{-23}$ J/K |
| $T_o$ | System Temperature | 300 K |
| $B_w$ | Channel Bandwidth | 80 MHz |
| $F$ | Noise Figure | 6 dB |

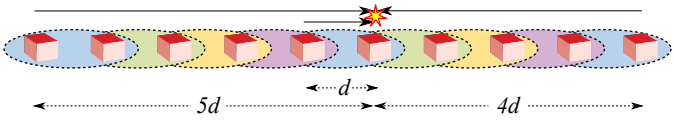


Fig. 2: Interference from the first tier of co-channel cells: The first set of interferers are located at distances of $5d$ and $6d$ respectively.

are given in Table I. Assuming a flat and open propagation environment, the path loss $L_{\text{FE}}$ can be characterized by the two-ray ground reflection model [11].

$$L_{\text{FE}}(d) = 4\left(\frac{c}{4\pi f d}\right)^2 \sin^2\left(\frac{4\pi f h^2}{d}\right) \tag{1}$$

Given the presence of co-channel interference, the signal-to-interference-plus-noise ratio (SINR) becomes an important metric that determines both the rate and reliability of data transfer. The impact of the first-tier of interference is illustrated in Fig. 2, assuming a total of 4 channels for the mesh network. The SINR in the worst-case scenario can be formulated under the influence of interference from the first three tiers of co-channel cells.

$$\text{SINR} = \frac{P_t G^2 L_{\text{FE}}(d)}{\eta + I} \tag{2}$$

$$\eta = k_B T_o B_w F \tag{3}$$

$$I = \sum_{i=1}^{3} P_t G^2 (L_{\text{FE}}(4id) + L_{\text{FE}}((4i+1)d)) \tag{4}$$

where $\eta$ is the thermal noise power and $I$ is the total interference power from the first 3 tiers of co-channel cells. For $n$ channels, $I$ may be generalized to $\sum\{L_{\text{FE}}(nid) + L_{\text{FE}}((ni+1)d)\}$ for i $\in$ {1,2,3}. A suitable value for $h$ can be chosen such that the SINR is maximized, for a given value of $d$.

While an IEEE 802.11ac mesh network may suffice at layer $\mathbf{L_2}$, its performance will not support the gigabit rates required at $\mathbf{L_3}$. For larger values of $R$, data transfer can only occur at lower modulation and coding scheme (MCS) indices. Hence, an IEEE 802.11ac mesh network is an undesirable choice for the bottleneck links in high-density seismic acquisition, contrary to the proposed 802.11ac-based schemes in [5], [6]. Moreover, a large latency at layer $\mathbf{L_3}$ would result in rapid buffering at the nodes, which can eventually lead to buffer overflows over time.

### *B. IEEE 802.11ac Mesh Network in Conjunction with UAVs*

UAVs provide a viable solution in challenging terrain where there are large obstacles or there is considerable difficulty in laying down equipment. Furthermore, in order to solve the aforementioned buffer overflow problem, the 802.11ac mesh network can be augmented with Unmanned Aerial Vehicles (UAVs) that cyclically visit each of the DCCRs. Given the small form factor at 60 GHz, the UAVs can be equipped with IEEE 802.11ad radios to rapidly collect data from the DCCRs at Gigabit rates. The IEEE 802.11ad standard operates over unlicensed spectrum in the 60 GHz bands [12], and can attain data rates of up to 7 Gbps over a channel bandwidth of 2.16 GHz. A line-of-sight (LoS) link can be established in a vertical orientation between a UAV and a DCCR, with a separation of a few meters. For instance, given a transmit power of 10 dBm, a realized antenna gain of 17 dB, and a separation distance of 5 m, the free-space path loss at 60 GHz translates to about 82 dB, yielding a received power of about -38 dBm. This is well above the minimum receiver sensitivity of -49 dBm to operate with an MCS index of 23 at a raw data rate of 6.237 Gbps [12].

Although the data transfer time may be minimal, the overall latency is predominantly determined by the physical movement of the UAVs over several kilometers. Hence, an inherent problem with the use of UAVs is an initial latency that ripples across subsequent sweeps.

We consider this scheme at the $\mathbf{L_3}$ layer only, since it may be impractical to deploy numerous UAVs at the $\mathbf{L_2}$ layer. Let $t_u$ represent the time taken by a UAV to traverse between adjacent DCCRs, and $t_d$ represent the time taken for each UAV to acquire all the buffered data from a DCCR.

$$t_u = \frac{1.5R}{v_{\text{avg}}} \tag{5}$$

$$t_d = \frac{B}{R_d} = \frac{R_b t_u}{R_d} \tag{6}$$

where $B$ is the buffered amount of data in each of the DCCRs prior to a forthcoming visit of a UAV, $R_d$ is the rate of data transfer over an IEEE 802.11ad link and $v_{\text{avg}}$ is the average velocity of the UAVs. The value of $B$ is dependent on $t_u$ since data is buffered at a UAV between two consecutive visits of the UAVs. Given that $R_b$ is the buffering rate at the DCCRs, the maximum value that $B$ will attain prior to the visit of a UAV is $R_b t_u$.

Let $N$ be the total number of DCCRs on one side of the DCC. Based on the value of $N$, the minimum required number of UAVs to ensure a regular cyclic movement can be expressed as $2kN$, where $k \geq 1$. As shown in Fig. 3a, a minimum of 2 UAVs for each of the intermediate DCCRs is required to ensure that data is delivered to the DCC at regular intervals of $(t_u + t_d)$. This duration can be reduced by employing a greater number of UAVs. For instance in Fig. 3b, when $k = 2$, the DCC is visited by UAVs at intervals of $(t_u + t_d)/2$. Assuming that data transfer occurs only for those UAVs moving toward the DCC, the total time for a UAV to complete a loop ($T_{\text{loop}}$) can be formulated.

$$T_{\text{loop}} = 2N\left(t_u + \frac{t_d}{k}\right) \tag{7}$$

$$= 2Nt_u\left(1 + \frac{R_b}{kR_d}\right) \tag{8}$$

$$= 2Nt_{\text{eff}} \tag{9}$$

where $t_{\text{eff}}$ is the effective time taken by a UAV to acquire data from a single DCCR and traverse to an adjacent one. Clearly, the total cycle time $T_{\text{loop}}$ can be minimized by ensuring that $kR_d >> R_b$.

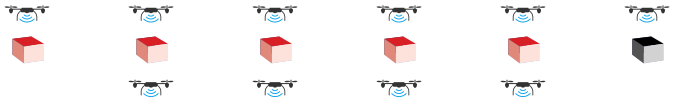

(a) Initial UAV pattern for $N = 5$ and $k = 1$.

(b) Initial UAV pattern for $N = 5$ and $k = 2$.

Fig. 3: Cyclic movement of UAVs at the $\mathbf{L_3}$ layer.

For the very first sweep, a minimum latency of $T_{\text{loop}}/2 = Nt_{\text{eff}}$ is observed. To minimize this initial latency, an IEEE 802.11ac mesh network may be used to transfer data to a DCCR that is a few hops away from the DCC, from where the relaying process is continued by a UAV. Hence, for $t < T_{\text{loop}}/2$, a combination of the 802.11ac mesh network and UAV rotation can be employed, and a value for the minimum initial latency can be formulated.

$$\text{Minimum Initial Latency} = \min\left\{\tau_i + it_{\text{eff}}, Nt_{\text{eff}}\right\} \quad (10)$$

where $\tau_i$, $1 \leq i \leq N-1$, denotes the time taken to transmit 1 sweep's worth of information to a DCCR that is $i$ hops away from the DCC. For $t \geq T_{\text{loop}}/2$, the regular cyclic movement of UAVs would take over the data transfer process.

Although a larger value for $v_{\text{avg}}$ or $k$ would result in smaller $t_{\text{eff}}$, which in turn can reduce the minimum latency in (10), the latency in the long term ($t >> T_{\text{loop}}/2$) would remain unaffected. Consider an expression for the seismic acquisition time lag (SATL) in the long term for the $p^{th}$ sweep.

$$\begin{aligned}
\text{SATL} &= \lim_{p\to\infty} \left\{T(p) - pT_{th}\right\}^+ && (11)\\
&= \lim_{p\to\infty} \left\{\left\lceil \frac{pS}{R_b t_{\text{eff}}} \right\rceil \cdot Nt_{\text{eff}} - pT_{th}\right\}^+ && (12)\\
&= \lim_{p\to\infty} \left\{\left(\frac{pS}{R_b t_{\text{eff}}}\right) \cdot Nt_{\text{eff}} - pT_{th}\right\}^+ && (13)\\
&= \lim_{p\to\infty} \; p\left\{\frac{NS}{R_b} - T_{th}\right\}^+ && (14)
\end{aligned}$$

where $T(p)$ denotes the time taken to acquire data corresponding to the $p^{th}$ sweep, $T_{th}$ is the time threshold for real-time acquisition, $S$ is the amount of data corresponding to a single sweep, $\lceil\cdot\rceil$ denotes the ceiling function, and $\{\alpha\}^+ = \alpha$ when $\alpha \geq 0$, else $\{\alpha\}^+ = 0$ when $\alpha < 0$. For a large value of $p$, $\lceil pS/R_b t_{\text{eff}}\rceil \approx pS/R_b t_{\text{eff}}$. Hence, the SATL is independent of $t_{\text{eff}}$, suggesting that it cannot be reduced by modifying $v_{\text{avg}}$ or $k$, and is determined by the $\mathbf{L_1}$ dependent parameters $R_b$ and $N$ alone.

### C. IEEE 802.11ad Mesh Network

A novel approach would be to utilize the geophones in an existing RL at the $\mathbf{L_3}$ layer, rather than deploying additional DCCRs. As for the $\mathbf{L_2}$ layer, additional geophones or relay devices would have to be deployed, which can take advantage of serving as additional sources of seismic data. The high-rate capability of the IEEE 802.11ad standard can be employed here, with each of the geophones being equipped with 802.11ad radios, and the static nature of the network can be exploited to perform the beamforming process only at the start of the seismic acquisition process.

TABLE II: Parameters for IEEE 802.11ad

| Symbol | Parameter | Value |
|---|---|---|
| $P_t$ | Transmit Power | 10 dBm |
| $G$ | Realized Antenna Gain | 17 dB |
| $f$ | Operating Frequency | 57-64 GHz |
| $h$ | Antenna Height | 0.1-1 m |
| $d$ | Distance between Adjacent Nodes | 25 m |
| $B_w$ | Channel Bandwidth | 2160 MHz |
| $F$ | Noise Figure | 10 dB |

A link budget analysis is undertaken to find the limits of operation for the given scenario. Consider a chain of geophones, separated by 25 m, operating over 4 channels. The various parameters are listed in Table II. The flat-Earth path loss model can be characterized using specific reflection coefficients $\Gamma_\perp$ in addition to the atmospheric absorption loss in the 60 GHz bands [13], [14].

$$L_{\text{FE}}(d) = \left(\frac{c}{4\pi f d}\right)^2 \left|1 + \Gamma_\perp e^{j4\pi f h^2/cd}\right|^2 \times 1.003922^{-d} \quad (15)$$

A straightforward computation of the received power $P_r$ reveals that such a link is feasible for an MCS index of 23.

$$P_r = P_t G^2 L_{\text{FE}}(25) \approx -46 \text{ dBm} \quad (16)$$

Furthermore, the SINR in the worst case scenario can also be shown to be sufficient for having reliable communication using an MCS index of 23.

$$\begin{aligned}
\text{SINR} &= \frac{P_t G^2 L_{\text{FE}}(d)}{\eta + I} && (17)\\
\eta &= k_B T_o B_w F && (18)\\
I &= \sum_{i=1}^{3} P_t G^2 (L_{\text{FE}}(4id) + L_{\text{FE}}((4i+1)d)) && (19)
\end{aligned}$$

An important problem that arises at higher layers of the Internet protocol stack is the use of the Transmission Control Protocol (TCP) over the proposed chain of geophones. It is known that TCP is not well-suited for mesh networks with a large number of hops, since an acknowledgment from the receiver may be delayed extensively, which in turn is interpreted as packet loss by the transmitter. This is exacerbated in the proposed scenario wherein the DCC can be 200-240 hops away from the farthest geophone, at layer $\mathbf{L_3}$. To circumvent this problem, 1-hop TCP links can be established between each pair of adjacent geophones, rather than having a dedicated link between each of the geophones and the DCC. Based on the amount of data received, the geophones can

accordingly update their respective TCP applications and relay the appropriate data segments.

### D. Free Space Optical (FSO) Mesh Network

FSO systems are an attractive option for deploying outdoor point-to-point links owing to a combination of high data rate capability and market penetration [15]. In the case of FSO systems, the total path loss can be expressed as a combination of various factors [15].

$$L_{\text{FSO}} = L_{\text{bd}} \cdot L_{\text{p}} \cdot L_{\text{o}} \cdot L_{\text{w}} \quad (20)$$

$$L_{\text{bd}} = \left(\frac{4}{\pi}\right)^2 \frac{A_t A_r}{\lambda^2 d^2} \quad (21)$$

where $L_{\text{bd}}$ is the beam divergence loss, $L_{\text{p}}$ is the pointing/misalignment loss, $L_{\text{o}}$ is the optics setup loss, and $L_{\text{w}}$ is the loss due to weather factors. $L_{\text{o}}$ is taken to be around 5 dB and given the static nature of the network, $L_{\text{p}} \approx 3$ dB. A suitable choice for $\lambda$ is 1550 nm since a large transmit power can be used without hampering eye safety and the transmission is more robust to background radiation noise. Given a beam divergence angle of 2 mrad, the transmit aperture diameter can be expressed as $(\lambda/\theta)$ [15], using which $A_t$ is determined. An industry-standard value of 150 mm can be chosen for the receiver aperture diameter. $L_{\text{bd}}$ can then be computed using (21). For a distance of 1400 m, $L_{\text{FSO}} \approx 33.5$ dB. The various parameters are listed in Table III. Given a minimum receiver sensitivity of $-23$ dBm for 2.5 Gbps links, a link margin value of 19.5 dB for weather effects can be assigned to $L_{\text{w}}$. While seismic surveys are typically not conducted in harsh weather conditions, this margin can ensure reliable operation under mild weather effects. Additional scintillation effects can be tackled via the use of coding and diversity techniques [15].

Another important metric for reliability is the signal-to-noise ratio (SNR) [15], [16].

$$\text{SNR} = \frac{(\gamma P_t L_{\text{FSO}})^2}{\sigma_n^2} \quad (22)$$

$$\sigma_n^2 = \sigma_{\text{shot}}^2 + \sigma_{\text{thermal}}^2 \quad (23)$$

where $\sigma_n^2$ is the noise variance. The various parameters for computing $\sigma_n^2$ can be found in [15], [16]. $\gamma$ is the responsivity of the photodetector, and has a value of 0.95 A/W for InGaAs photodetectors at 1550 nm wavelength [15]. Overall, feasible FSO links at 2.5 Gbps can be set up for acquiring seismic data at layers $\mathbf{L_2}$ and $\mathbf{L_3}$, provided that LoS propagation exists between the relay nodes.

TABLE III: Parameters for FSO links

| Symbol | Parameter | Value |
|---|---|---|
| $P_t$ | Transmit Power | 30 dBm |
| $\lambda$ | Operating Wavelength | 1550 nm |
| $d$ | Distance between Adjacent Nodes | 300-1400 m |
| $\theta$ | Beam Divergence | 2 mrad |
| $A_t$ | Transmitter Aperture Area | $4.717 \times 10^{-7}$ m$^2$ |
| $A_r$ | Receiver Aperture Area | $1.767 \times 10^{-2}$ m$^2$ |

## IV. Performance Evaluation

The ns-3 simulator is used for comparing the performance exhibited by the IEEE 802.11ac standard, as suggested in prior works [5], [6], and the proposed approaches using UAVs, the IEEE 802.11ad standard, and FSO systems. Simulation parameters are derived from Tables I-III. Considering that $\mathcal{L} = 6$ s and $\mathcal{S} = 8$ s, the value of $T_{th} = \mathcal{L} + \mathcal{S} = 14$ s, using which the SATL can be computed in (11). For the sake of analysis, the $\mathbf{L_1}$-*Latency Rate (LLR)* is defined to be the average rate at which the latency with the respect to the $\mathbf{L_1}$ layer, grows with time. A large and finite value for the LLR would hinder real-time acquisition for a large number of sweeps. The performance is evaluated after fixing the WGN range parameter ($R$) at the $\mathbf{L_1}$ layer. For $R = 300$ m, the acquisition time lag introduced by the $\mathbf{L_1}$ layer is 0, whereas in the case of $R = 600$ m, there is an inherent lag of about 5 s per sweep [8]. This would help determine whether a large SATL arises from the $\mathbf{L_1}$ or $\mathbf{L_3}$ layers, and in turn gauge which layer forms the bottleneck of the architecture.

The overall performance of the various schemes at the $\mathbf{L_2}$ layer is shown in Fig. 4. In Fig. 4a, the LLR is negligible for the 802.11ad and FSO schemes, suggesting that real-time acquisition is achievable even for a large number of sweeps. However, the 802.11ac standard is unable to sustain a minimal LLR for $R > 550$ m, owing to a sudden drop in the MCS index that can reliably be used. This is also reflected in the average buffer size, shown in Fig. 4b. For $R = 600$ m, the average buffer size grows exponentially with time, leading to a buffer flow at the WGNs in the long run. A quantitative analysis for the SATL reveals that while all the schemes are able to support real-time acquisition for $R = 300$ m, a finite lag is introduced for $R = 600$ m. In the case of the 802.11ad and FSO schemes, the lag is introduced by the underlying $\mathbf{L_1}$ layer, while the lag is initially higher in the case of 802.11ac due to the additional impediment of its high LLR but tends to converge at the lag dictated by the $\mathbf{L_1}$ layer for later sweeps.

At the topmost $\mathbf{L_3}$ layer, the overall performance is exacerbated by the need for higher data rates. In Fig. 5a, the 802.11ac and UAV-based schemes suffer from a finite and large LLR. Its impact is seen in Fig. 5b where the average buffer size grows exponentially with time. However, the buffer overflow problem is rectified by the UAV-based scheme wherein the buffer is flushed at regular intervals. Meanwhile, the 802.11ad and FSO schemes perform well under the conditions imposed by the $\mathbf{L_3}$ layer as well. For the case when $R = 300$ m, the SATL for the 802.11ac scheme grows exponentially as a consequence of a high LLR. As for the UAV-based scheme, a large value of SATL is perceived initially, as given by (10), after which it converges to around 0 in the long term. For $R = 600$ m, the SATL for the 802.11ac and UAV-based schemes grow exponentially, as a result of high LLR and a large value for (SATL/$p$) in (14) respectively. The 802.11ad and FSO schemes sustain minimal LLR, but nevertheless suffer a finite SATL that is introduced by the $\mathbf{L_1}$ layer.

The power consumption parameters are derived from [9],

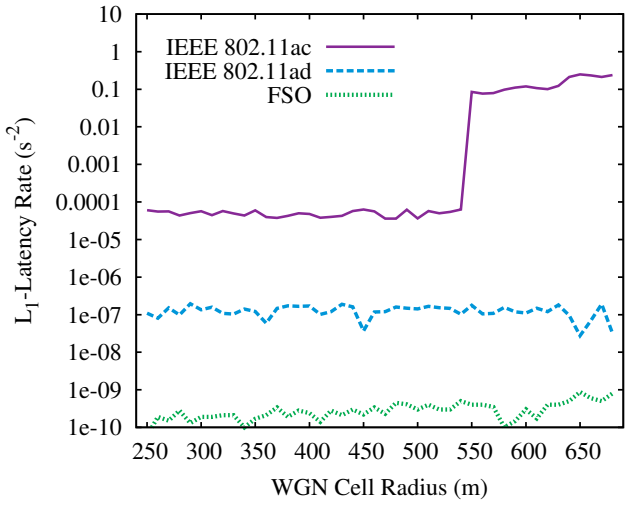


(a) Latency with respect to Layer $\mathbf{L_1}$

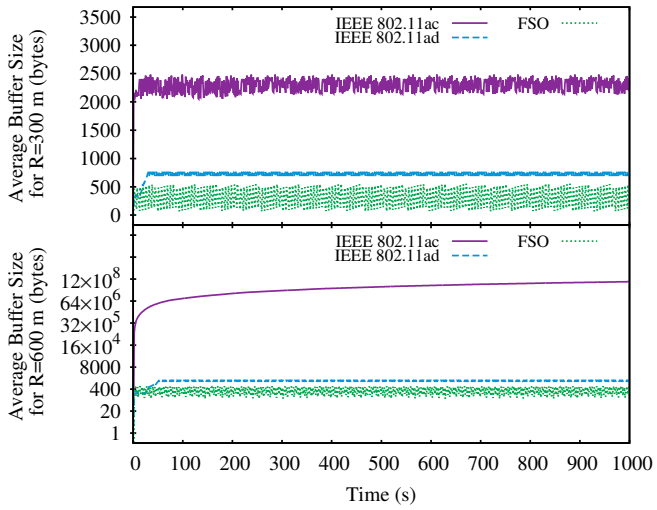


(b) Average Buffer Size at Relay Nodes

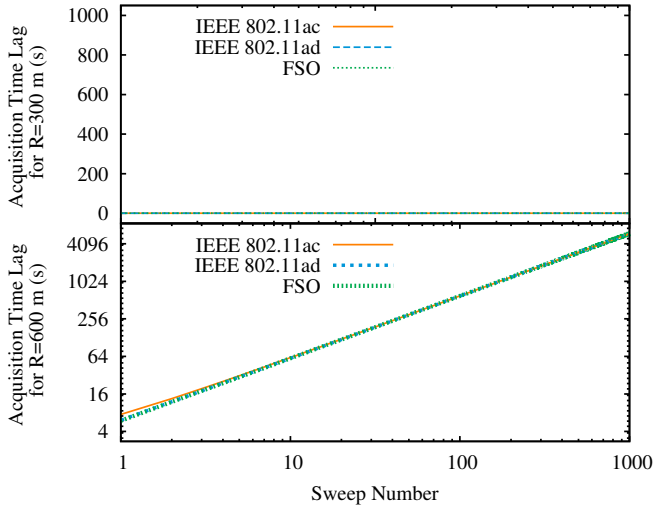


(c) Seimic Acquisition Time Lag up to 1000 sweeps

Fig. 4: Performance Evaluation at Layer $\mathbf{L_2}$

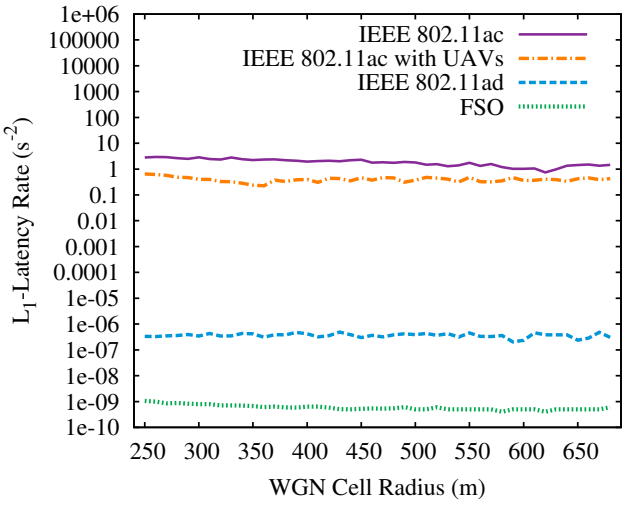


(a) Latency with respect to Layer $\mathbf{L_1}$

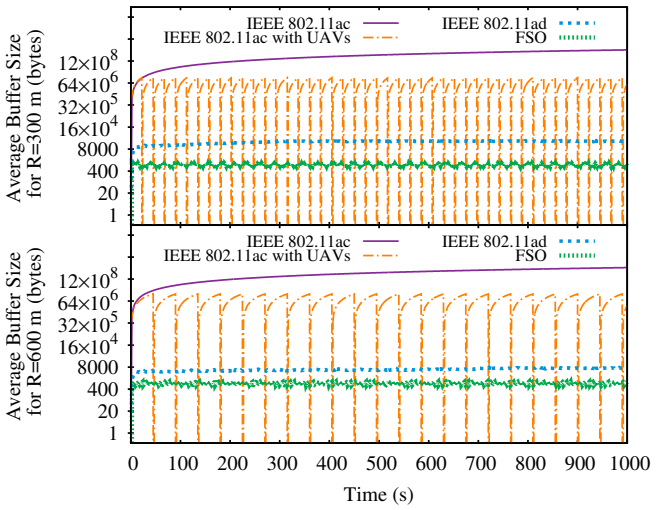


(b) Average Buffer Size at Relay Nodes

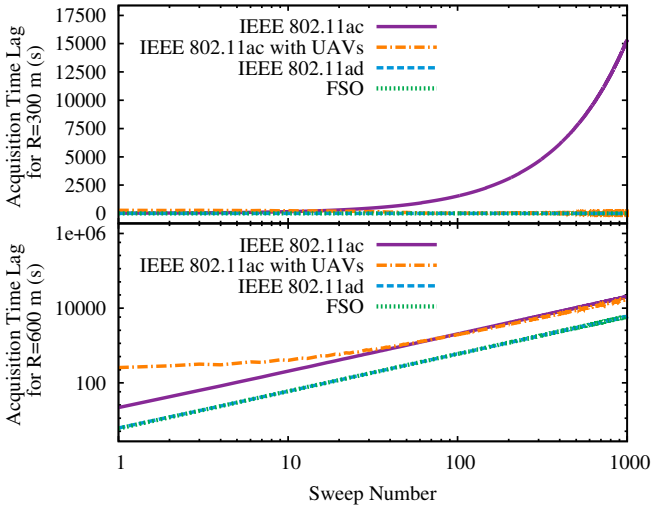


(c) Seimic Acquisition Time Lag up to 1000 sweeps

Fig. 5: Performance Evaluation at Layer $\mathbf{L_3}$

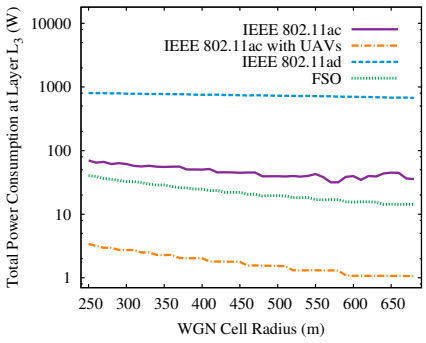


(a) Total Power Consumption

| Scheme | | Average Seismic Acquisition Time Lag Per Sweep (s) | | | | | | |
|---|---|---|---|---|---|---|---|---|
| $\mathbf{L_2}$ | $\mathbf{L_3}$ | 0s | $(0, 7]$ | $(7, 14]$ | $(14, 21]$ | $(21, 28]$ | $(28, 35]$ | $(35, 42]$ |
| 802.11ac | 802.11ac | ✗ | ✗ | ✗ | $W \geq 84$ | $W \geq 84$ | $W \geq 78$ | $W \geq 66$ |
| 802.11ac | 802.11ac/UAV | $W \geq 275$ | $W \geq 230$ | $W \geq 199$ | ✗ | ✗ | $W \geq 180$ | ✗ |
| 802.11ac | 802.11ad | $W \geq 144$ | $W \geq 91$ | $W \geq 78$ | $W \geq 66$ | ✗ | ✗ | ✗ |
| 802.11ac | FSO | $W \geq 144$ | $W \geq 91$ | $W \geq 78$ | $W \geq 66$ | ✗ | ✗ | ✗ |
| 802.11ad | 802.11ac | ✗ | ✗ | ✗ | $W \geq 84$ | $W \geq 84$ | $W \geq 66$ | $W \geq 66$ |
| 802.11ad | 802.11ac/UAV | $W \geq 275$ | $W \geq 230$ | $W \geq 199$ | ✗ | ✗ | $W \geq 180$ | ✗ |
| 802.11ad | 802.11ad | $W \geq 144$ | $W \geq 84$ | $W \geq 66$ | $W \geq 66$ | ✗ | ✗ | ✗ |
| 802.11ad | FSO | $W \geq 144$ | $W \geq 84$ | $W \geq 66$ | $W \geq 66$ | ✗ | ✗ | ✗ |
| FSO | 802.11ac | ✗ | ✗ | ✗ | $W \geq 84$ | $W \geq 84$ | $W \geq 66$ | $W \geq 66$ |
| FSO | 802.11ac/UAV | $W \geq 275$ | $W \geq 230$ | $W \geq 199$ | ✗ | ✗ | $W \geq 180$ | ✗ |
| FSO | 802.11ad | $W \geq 144$ | $W \geq 84$ | $W \geq 66$ | $W \geq 66$ | ✗ | ✗ | ✗ |
| FSO | FSO | $W \geq 144$ | $W \geq 84$ | $W \geq 66$ | $W \geq 66$ | ✗ | ✗ | ✗ |

(b) Minimum Number of Required WGNs as a function of intervals of the Average SATL per Sweep.

Fig. 6: Additional Metrics for Performance Evaluation

[17], [18] and the performance exhibited by the various approaches is shown in Fig. 6a. Power consumption is evaluated only for the relay devices and geophones that require manual recharging, contrary to devices such as the UAVs that can be recharged autonomously. A high power consumption for the 802.11ad approach arises from the use of a large channel bandwidth and from the need for a large number of radios along a chain of geophones. The 802.11ac and FSO schemes are more power-efficient, with FSO equipment consuming lesser power than typical RF systems [15], [18]. The power consumption is least via the UAV approach since the relay nodes only have to perform data transfer upon the visit of a UAV. The overall trend for all schemes is a decreasing one since $N$ decreases with increasing $R$.

In Fig. 6b, the minimum number of required WGNs ($W$) at the $\mathbf{L_1}$ layer is computed [8] for all possible combinations of the backhaul strategies at the $\mathbf{L_2}$ and $\mathbf{L_3}$ layers, as a function of the average seismic acquisition time lag per sweep (SATL/$p$). As expected, the 802.11ad and FSO schemes perform best while delivering real-time acquisition with $W \geq 144$. $W$ is reduced to just 66 when an average SATL of 14-21 s can be tolerated per sweep, suggesting that the bottleneck has been shifted to the $\mathbf{L_1}$ layer. Meanwhile, employing the 802.11ac scheme at layer $\mathbf{L_3}$ can only operate with a minimum lag of 14 s per sweep, as a consequence of its high LLR. Although the UAV-based scheme can solve the buffer overflow problem in the 802.11ac scheme, its overall performance is inferior to the 802.11ad and FSO schemes.

## V. Conclusion

Various wireless backhaul strategies based on the use of UAVs, the IEEE 802.11ac and IEEE 802.11ad standards, and FSO systems have been proposed and evaluated from the seismic acquisition perspective. The proposed wireless geophone network architecture can tackle with the obstacles presented in a seismic survey, while sustaining real-time acquisition with a minimal number of gateways. Moreover, the antenna heights can be chosen so as to minimize both the co-channel interference and the related logistics cost. Each of the proposed schemes has its pros and cons, which can be exploited as per the seismic survey area terrain and requirements. Overall, the proposed architecture can be incorporated into high-density seismic surveys to achieve seamless real-time acquisition.

## References


[1] G. Vermeer, *3D Seismic Survey Design*, 2nd ed. Society of Exploration Geophysicists, 2012.

[2] C. Bagaini, T. Bunting, A. El-Emam, A. Laake, and C. Strobbia, "Land seismic techniques for high-quality data," *Oilfield Review*, vol. 22, no. 2, 2010.

[3] D. Crice, "The state of land seismic," *First Break*, vol. 36, no. 1, pp. 65–67, 2014.

[4] C. Rosa, M. Kuusela, F. Frederiksen, and K. I. Pedersen, "Standalone LTE in Unlicensed Spectrum: Radio Challenges, Solutions, and Performance of MulteFire," *IEEE Communications Magazine*, vol. 56, no. 10, pp. 170–177, OCTOBER 2018.

[5] S. Savazzi, U. Spagnolini, L. Goratti, D. Molteni, M. Latva-aho, and M. Nicoli, "Ultra-wide band sensor networks in oil and gas explorations," *IEEE Communications Magazine*, vol. 51, no. 4, pp. 150–160, April 2013.

[6] D. Crice, "A Cable-Free Land Seismic System that Acquires Data in Real Time," *First Break*, vol. 32, no. 1, pp. 97–100, 2014.

[7] V. A. Reddy, G. L. Stüber, and S. Al-Dharrab, "Energy Efficient Network Architecture for Seismic Data Acquisition via Wireless Geophones," in *IEEE International Conference on Communications (ICC)*, Kansas City, USA, May 2018.

[8] V. A. Reddy, G. L. Stüber, S. Al-Dharrab, W. Mesbah, and A. H. Muqaibel, "A Wireless Geophone Network Architecture Using IEEE 802.11af With Power Saving Schemes," *IEEE Transactions on Wireless Communications*, vol. 18, no. 12, pp. 5967–5982, Dec 2019.

[9] V. A. Reddy, G. L. Stüber, and S. I. Al-Dharrab, "High-Speed Seismic Data Acquisition Over mm-Wave Channels," in *2018 IEEE 88th Vehicular Technology Conference (VTC-Fall)*, Aug 2018, pp. 1–5.

[10] "IEEE 802.11ac, Amendment 4: Enhancements for Very High Throughput for Operation in Bands below 6 GHz," pp. 1–425, Dec 2013.

[11] G. L. Stüber, *Principles of Mobile Communication*, 4th ed. Springer International Publishing, 2017.

[12] "IEEE 802.11ad, Amendment 3: Enhancements for Very High Throughput in the 60 GHz Band," pp. 1–628, Dec 2012.

[13] S. Jaeckel, L. Raschkowski, S. Wu, L. Thiele, and W. Keusgen, "An explicit ground reflection model for mm-wave channels," in *2017 IEEE Wireless Communications and Networking Conference Workshops*, March 2017, pp. 1–5.

[14] ITU-R P.676-11, "Attenuation by atmospheric gases," *Tech. Rep.*, 2016.

[15] Z. Ghassemlooy, W. Popoola, and S. Rajbhandari, *Optical Wireless Communications: System and Channel Modelling with MATLAB*. CRC Press, Inc., 2012.

[16] J. M. Kahn and J. R. Barry, "Wireless infrared communications," *Proceedings of the IEEE*, vol. 85, no. 2, pp. 265–298, Feb 1997.

[17] Y. Zeng, P. H. Pathak, and P. Mohapatra, "A First Look at 802.11ac in Action: Energy Efficiency and Interference Characterization," in *2014 IFIP Networking Conference*, June 2014, pp. 1–9.

[18] S. Deng, J. Liao, Z. R. Huang, M. Hella, and K. Connor, "Wireless connections of sensor network using RF and free space optical links," in *Next-Generation Communication and Sensor Networks*, Sept 2007.